Transition Metal Chemistry (2019) 44:555–564
https://doi.org/10.1007/s11243-019-00312-8

Double-shell structural polyaniline-derived TiO_2 hollow spheres for enhanced photocatalytic activity

Xuefeng Sun[1] · Bin Sun[1] · Qinghua Gong[1] · Tingting Gao[1] · Guowei Zhou[1]

Received: 5 November 2018 / Accepted: 19 February 2019 / Published online: 6 March 2019

Abstract
Polyaniline (PANI) is a conducting polymer which has been employed as a photosensitizer for enhancing the performance of a number of photocatalysts. Herein, we describe the synthesis of organic–inorganic hybrid materials in order to enhance the photocatalytic activity of double-shell TiO_2/PANI hollow spheres (TAHSs), which were fabricated by means of sol–gel and in situ polymerization processes. The physicochemical properties of the PANI-modified TiO_2 hollow spheres were investigated by a variety of techniques. The effect of the PANI shell layer on the photocatalytic activity of TAHSs was elucidated. With the optimal PANI content, the resultant TiO_2/PANI hybrid materials exhibited remarkably enhanced UV and visible light photocatalytic degradation of aqueous methyl orange, far exceeding the activity of bare TiO_2 hollow spheres. The synergistic effect between TiO_2 and PANI is explained in terms of the improved separation of photogenerated electron–hole pairs.

Introduction

Titanium dioxide, as a typical semiconducting metal oxide, has attracted much interest in recent decades thanks to its low cost, low toxicity, excellent chemical stability, and environmentally benign nature [1, 2]. To date, many morphologies including TiO_2 nanorods, nanowires, nanotubes, nanosheets, and hollow spheres [3–7], have been synthesized by a variety of methods. Among the diverse range of TiO_2 morphologies, hollow spheres have attracted extensive interest based on their superior properties, including large surface area, low density, and high light-harvesting efficiency [8, 9].

Previous studies have included extensive investigations of TiO_2 within the contexts of photocatalysis [10], power conservation [11], photoelectric devices [12, 13], etc. Yet, the band gap (E_g = 3.2 eV) of TiO_2 is so wide that its capacity for light absorption extends only as far as the UV region, which seriously limits its widespread application. Moreover, the application of TiO_2 as a photocatalyst is also restricted by the low separation rate of the photogenerated charge carriers [14]. In the light of these issues, many approaches have been explored with a view to improve the photocatalytic performance of TiO_2, especially by the construction of hybrid materials. Thus, hybrid materials such as NiO/TiO_2 [15], g-C_3N_4/TiO_2 [16], rGO/TiO_2 [17] and so on can extend the light absorption of TiO_2 into the visible range and inhibit the recombination of photogenerated electrons and holes, contributing to a significant enhancement of photocatalytic performance. In recent years, conducting polymers have been used as promising photosensitizers for TiO_2 photocatalysts, by virtue of their spatially extended π conjugation [18]. Hybrid materials composed of TiO_2 modified with conducting polymers have been reported to shift its spectral response into the visible light range [19]. In this context, PANI is a well-known conducting polymer with a narrow forbidden band gap, high absorption coefficients and migration rates of electrons, which has been identified as a candidate for TiO_2 sensitization [20]. Therefore, TiO_2/PANI hybrid materials have aroused much interest in photocatalysis research [21]. To date, PANI-modified TiO_2 nanomaterials with various morphologies have been synthesized, including nanotubes [22], nanowires [23], nanorods [24], and so on. However, to the best of our knowledge, there are few reports of double-shell structural TiO_2/PANI hollow spheres

Electronic supplementary material The online version of this article (https://doi.org/10.1007/s11243-019-00312-8) contains supplementary material, which is available to authorized users.

✉ Bin Sun
binsun@qlu.edu.cn

✉ Guowei Zhou
gwzhou@qlu.edu.cn

[1] Key Laboratory of Fine Chemicals in Universities of Shandong, School of Chemistry and Pharmaceutical Engineering, Qilu University of Technology (Shandong Academy of Sciences), Jinan 250353, People's Republic of China

with adjustable shell thickness. Combining the properties of PANI and TiO_2 hollow spheres, this unique architecture of the double-shell structural TiO_2/PANI hollow spheres affords more active sites, wider light absorption range, and faster matter transfer capability during photocatalysis [25].

Taking advantage of the photosensitive performance of PANI, we demonstrate in this study the photocatalytic activity of double-shell structural TiO_2/PANI hollow spheres that were synthesized via sol–gel and in situ polymerization processes. The PANI layer can be uniformly distributed on the surface of the TiO_2 hollow spheres, which is regarded as an important consideration in photocatalytic activity. Compared with bare TiO_2 hollow spheres, the TiO_2/PANI hybrid materials can inhibit the recombination of photogenerated charge carriers and remarkably enhance the photocatalytic degradation of methyl orange (MO) under both UV and visible light. A reasonable mechanism for the photocatalytic degradation of MO by this hybrid material is proposed.

Experimental section

Starting materials

The starting materials used in this study can be found in the Supplementary material.

Preparation of TiO_2/PANI hollow spheres

Precursor TiO_2 hollow spheres were obtained from SiO_2 and SiO_2/TiO_2 with subsequent etching, as described in the Supplementary material. For the preparation of TiO_2/PANI hollow spheres, TiO_2 (0.02 g) and polyvinylpyrrolidone (0.1 g) were injected into deionized water (25 mL) under ultrasonication. After ultrasonic irradiation 30 min at room temperature, an appropriate amount of aniline (ANI) and hydrochloric acid (200 µL, 37%) was added to the suspension and the mixture was stirred for 30 min. Next, the corresponding amount of ammonium persulphate (APS) (molar ratio of ANI/APS = 1:1) was added and stirring was continued for 10 h at ambient temperature. Finally, the solid was isolated by centrifugation, washed, and dried at 50 °C for 12 h. The amount of ANI in the suspension was adjusted to 1, 5, 10, and 15 µL, and the resulting products were designated as TAHSs-1, TAHSs-2, TAHSs-3, and TAHSs-4, respectively. For comparison, a bare PANI sample without any TiO_2 was also prepared under the same experimental conditions.

Characterization

The characterization techniques are listed in the Supplementary material.

Photocatalytic performance tests

The photocatalytic performance of the test samples was assayed by the photodegradation of MO under a 375 W high-pressure mercury lamp or a 500 W xenon lamp equipped with one UV cutoff filter ($\lambda \geq 420$ nm). Typically, 50 mg of photocatalyst was added to 100 mL of aqueous MO (10 mg L^{-1}) in a quartz reactor. Prior to irradiation, the suspension was kept in the dark for 30 min to allow for equilibration. The MO concentration was monitored with a UV–Vis spectrophotometer (Shimadzu UV-2550).

Results and discussion

Formation and morphology of the nanospheres

The synthesis of the TiO_2/PANI hollow spheres is outlined in Scheme 1. SiO_2 spheres were first prepared by Stöber's method, followed by hydrolysis of tetrabutyl titanate (TBT) on the surface of the SiO_2 spheres by a sol–gel method. The resulting core/shell SiO_2/TiO_2 materials were calcined, and then the SiO_2 template was removed by etching with NaOH solution to give TiO_2 hollow spheres. Finally, the PANI layer was coated onto the TiO_2 surface by in situ polymerization of ANI, giving the double-shell structural TiO_2/PANI hollow spheres. The corresponding TEM and SEM images are displayed in Figs. 1, S1, S2, and S3.

Figure 1a, b illustrates the formation of monodisperse SiO_2 spheres that are ~ 280 nm in diameter. By adjusting the amount of TBT (0.25, 0.5, and 0.75 mL), the thickness of the shell for SiO_2/TiO_2 and TiO_2 hollow spheres can be selected as ~ 12, 20, or 50 nm, respectively, as shown in Fig. S1 and Fig. 1c–f. Using the 50-nm-thick TiO_2 hollow spheres, it is distinctly seen that double-shell structural TiO_2/PANI hollow spheres (sample TAHSs-3) are constructed, as shown in Fig. 1g, h. The outer surface of the TiO_2/PANI hollow spheres is rougher compared with that of bare TiO_2 hollow spheres. The thickness of the PANI layer in the TiO_2/PANI hollow spheres is ~ 16 nm. Furthermore, double-shell structural TiO_2/PANI hollow spheres with different thicknesses of the PANI layer can be prepared by changing the amount of ANI (Fig. S2);

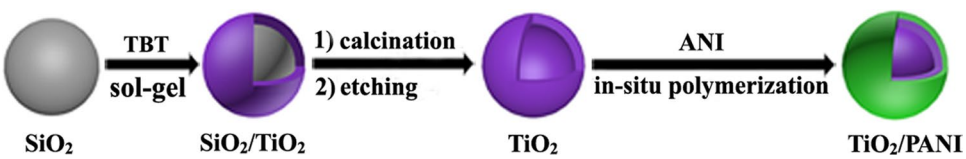

Scheme 1 Synthesis of double-shell TiO_2/PANI hollow spheres

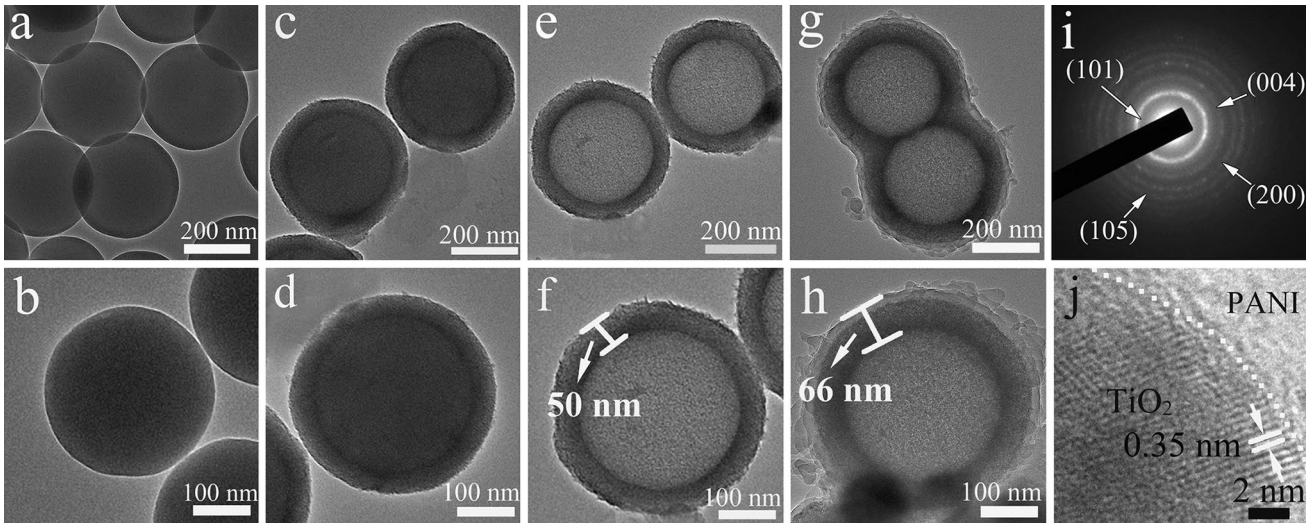

Fig. 1 TEM images of **a**, **b** SiO_2, **c**, **d** SiO_2/TiO_2, **e**, **f** TiO_2 hollow spheres, and **g**, **h** TAHSs-3; **i** SAED and **j** HRTEM of TAHSs-3

the shell thickness of PANI is estimated to be 5, 8, and 20 nm for samples TAHSs-1, TAHSs-2, and TAHSs-4, respectively. The selected area electron diffraction (SAED) pattern of TAHSs-3 reveals the (101), (004), (200), and (105) diffraction rings (Fig. 1i) characteristic of crystalline anatase TiO_2. The SAED of PANI is difficult to examine due to the amorphous structure. Figure 1j shows an HRTEM image of TAHSs-3; the fringe spacing is about 0.35 nm, which is consistent with the (101) lattice spacing of anatase TiO_2. Moreover, there is a layer of amorphous structure on the surface of the TiO_2 hollow spheres, which can be identified as the PANI layer, as reported by other research groups [26].

SEM images of the TiO_2 hollow spheres and double-shell TiO_2/PANI hollow spheres (represented by TAHSs-3) are shown in Fig. S3. From Fig. S3a, b, it can be seen that monodispersed TiO_2 hollow spheres are obtained with a mean diameter of ~ 380 nm, consistent with the TEM observations. Moreover, the cavity structure in Fig. S3a can clearly be observed for a broken TiO_2 sphere, providing powerful evidence that the TiO_2 hollow spheres are successfully prepared. Compared with the TiO_2 hollow spheres, the surface of the as-prepared TAHSs-3 (Fig. S3c, d) is extremely fuzzy and possesses a diameter of ~ 410 nm. Further observation shows that the dispersibility of TAHSs-3 is inferior than that of the TiO_2 hollow spheres, suggesting that PANI is liable to aggregation during the polymerization process.

Physicochemical performance

The crystalline structures of the TiO_2 hollow spheres, TiO_2/PANI hollow spheres, and PANI were investigated by XRD, as presented in Fig. 2A. For bare TiO_2 hollow spheres [Fig. 2A(a)], all of the diffraction peaks are identified with anatase TiO_2. The associated 2θ values of approximately 25.4, 37.9, 48.1, 54.6, 63.2, 69.8, and 75.4° can be unambiguously allocated to the (101), (004), (200), (105), (204), (116), and (215) crystal planes, respectively [15, 27]. The XRD pattern of bare PANI [Fig. 2A(f)] exhibits a broad reflection peaks located at 20° and 25°, corresponding to the parallel and perpendicular periodicity of the polymer chains, respectively [28]. However, the XRD pattern of PANI is negligible in the TiO_2/PANI hybrid materials [Fig. 2A(b–e)], which show only the diffraction peaks of anatase TiO_2. This may be related to the amorphous nature of PANI, together with the inhibition of a periodic structure in TiO_2/PANI hybrid materials [29]. It should be noted that the relative diffraction peaks of TiO_2 decrease with increasing thickness of the PANI layer, again suggesting that TiO_2/PANI hybrid materials are successfully constructed. The crystallite sizes of the samples were obtained by applying the Scherrer equation ($D = 0.9\lambda/\beta\cos\theta$, where D, λ, β, and θ are the average crystallite size, the wavelength of the X-ray radiation, the FWHM of the diffraction peak, and the peak position, respectively) to the anatase (101) diffraction peaks. The related values for the TiO_2 hollow spheres, TAHSs-1, TAHSs-2, TAHSs-3, and TAHSs-4 were determined as 13.18, 11.27, 10.68, 12.56, and 12.59 nm, respectively. The reduction of the crystallite sizes for the TAHSs samples can be attributed to the coating of PANI on the surface of the TiO_2 hollow spheres [30, 31].

Raman spectroscopy is a very sensitive tool for distinguishing different phase structures of nanomaterials by different space groups and is widely used in the field of nanomaterials [32]. Raman spectra of pure PANI, TiO_2 hollow spheres, and TiO_2/PANI hybrid materials are shown in Fig. 2B. The four characteristic peaks located at 147, 397,

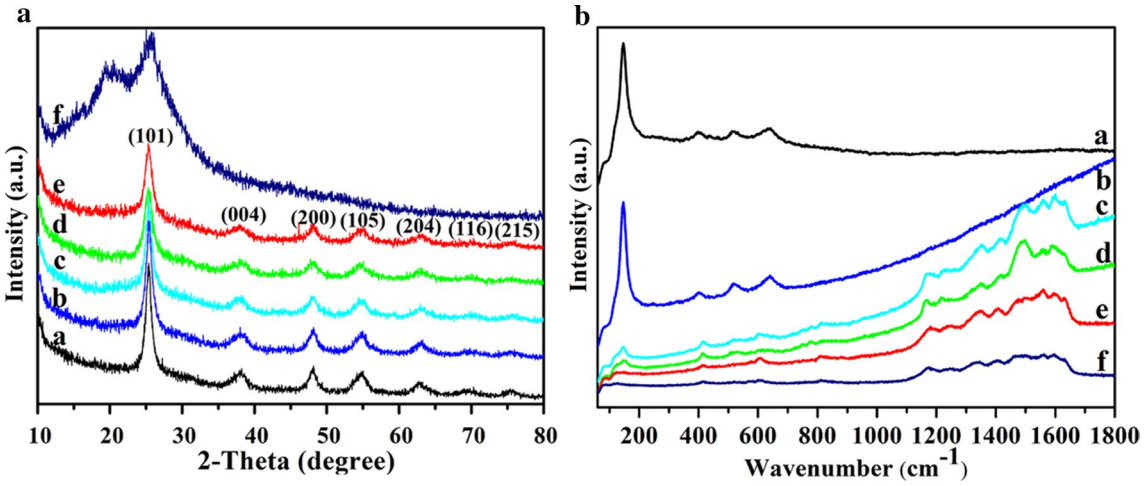

Fig. 2 **A** XRD patterns and **B** Raman spectra of (a) TiO_2 hollow spheres, (b) TAHSs-1, (c) TAHSs-2, (d) TAHSs-3, (e) TAHSs-4, and (f) PANI

520, and 638 cm^{-1} are characteristic of anatase TiO_2 and are assigned to the E_g phonon, B_{1g}, A_{1g}, and E_g modes of vibration, respectively [14], as shown in Fig. 2B(a). From Fig. 2B(f), the characteristic peaks of PANI at about 411, 604, and 811 cm^{-1} are assigned to C–H deformations, whilst distinct bands at 1181, 1348, 1407, 1557, and 1630 cm^{-1} are attributed to the C–H bending vibrations of the benzenoid or quinoid rings, $C–N^+$ stretch, C–C stretch, C=C stretches of the benzenoid ring, and benzenoid or quinonoid ring bending vibrations, respectively. The TiO_2 hollow spheres coated with PANI show weaker characteristic peaks of TiO_2, which can be explained by the PANI weakening the polarizability of the TiO_2 structure. Conversely, the characteristic peaks of PANI are significantly enhanced by the presence of TiO_2, similar to previously reported results [33]. These observations suggest an intense interaction between PANI and TiO_2 in the hybrid materials.

The chemical structure of the hybrids was investigated further by FT-IR analysis, as shown in Fig. S4. Compared with bare TiO_2 (Fig. S4a) and pure PANI (Fig. S4f), all the primary characteristic peaks of both PANI and TiO_2 can be found in the spectra of a series of TiO_2/PANI hybrid materials [Fig. S4(b–e)]. The peaks below 1000 cm^{-1} are related to Ti–O and Ti–O–Ti stretching modes [1, 34]. A broad peak at about 3400 cm^{-1} arises from the stretching vibrations of O–H and N–H groups on the surface of TiO_2 and in the PANI chains [35], whilst a peak at 1636 cm^{-1} corresponds to the O–H bending of adsorbed water molecules. The C=N and C=C stretches of the quinonoid and benzenoid units are observed at 1540 and 1489 cm^{-1}. The peaks at 1295 and 1210 cm^{-1} are assigned to C–N stretching modes of the benzenoid unit [36]. In addition, a peak at 1120 cm^{-1} is attributed to bending vibrations of C–H groups within PANI [29]. As the thickness of the PANI layer is increased, the broad peak assigned to O–H and N–H stretching shows a blue shift, suggesting that the interactions between PANI and TiO_2 hollow spheres are becoming stronger [37].

TGA curves of TiO_2 hollow spheres and the TiO_2/PANI hybrid materials are shown in Fig. S5. Two major weight losses are clearly seen in the TGA curves of the TiO_2/PANI hybrids. An initial weight loss is observed from room temperature to 320 °C and is attributed to the loss of water [38]; the second weight loss observed between 320 and 800 °C is associated with thermal decomposition of the PANI chains [39]. Overall weight losses of about 4.1, 6.2, 10.9, and 14.8% are observed for TAHSs-1, TAHSs-2, TAHSs-3, and TAHSs-4, respectively. For the pure TiO_2 hollow spheres, weight loss is only observed at temperatures below 320 °C, showing that TiO_2 is thermally stable above this temperature.

Figure S6 depicts the N_2 adsorption–desorption isotherms of the samples, which can be classified as typical IV isotherms with hysteresis loops according to IUPAC conventions [40], indicating the existence of mesoporous structure in both the TiO_2 hollow spheres and TiO_2/PANI hybrids. The specific surface areas were determined as 96, 83, 77, 72, and 64 $m^2\ g^{-1}$ for TiO_2 hollow spheres, TAHSs-1, TAHSs-2, TAHSs-3, and TAHSs-4, respectively. Hence, it can be clearly seen that the TiO_2 hollow spheres possess a larger specific surface area than the TiO_2/PANI hybrid materials. Moreover, the specific surface areas of the TiO_2/PANI hybrid materials diminish with increasing amounts of PANI.

As shown in Fig. 3, the chemical compositions and bonding nature of the TiO_2/PANI hybrid materials (TAHSs-3) were also investigated by XPS analysis. As shown in Fig. 3a, the elements C, O, N, and Ti are all present in the samples. Figure 3b shows the XPS survey spectrum of Ti at binding energies of 458.28 and 464.02 eV, corresponding to the Ti $2p_{2/3}$ and Ti $2p_{1/2}$ levels, respectively [41]. Figure 3c shows the O 1*s* spectrum at binding energies of 529.58 and

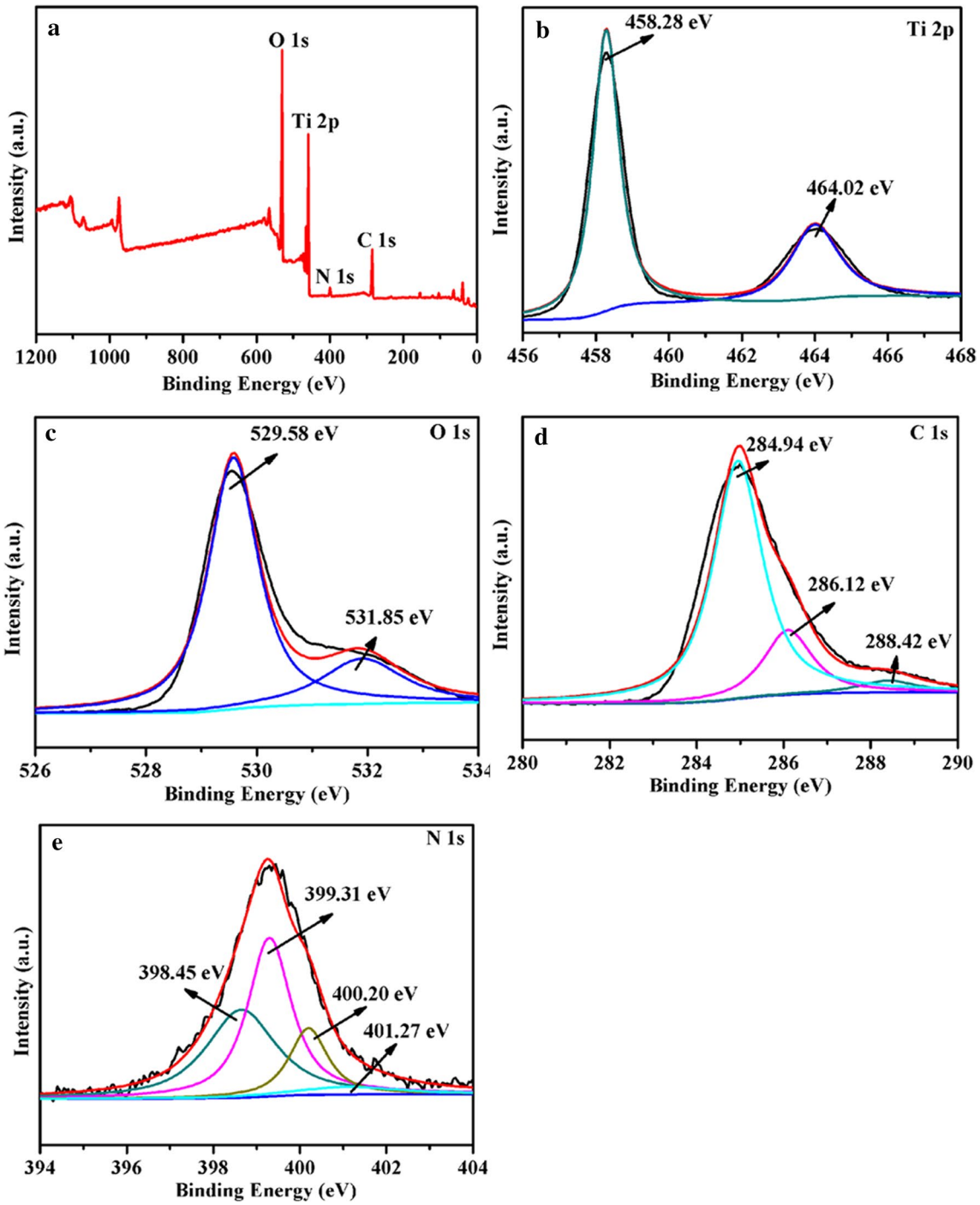

Fig. 3 XPS spectra of the TAHSs-3: **a** survey spectrum, **b** Ti 2*p*, **c** O 1*s*, **d** C 1*s*, and **e** N 1*s*

531.85 eV, resulting from Ti–O–Ti and hydrogen bonding within PANI and TiO_2 [26]. The binding energy values of the C 1*s* level in Fig. 3d are 284.94, 286.12 and 288.42 eV, corresponding to C–C and C=C, C–O–Ti, and C=O moieties [42]. Figure 3e shows the N 1*s* spectrum; it has four binding energies. The peaks at 398.45 and 400.20 eV are ascribed to pyridinic N and pyrrolic N. The interaction of N^+ and protons from the acid doping gives a peak at 401.27 eV, whilst metal–nitrogen bonds (M–N) are observed at 399.31 eV [43]. The identification of C–O–Ti and M–N bonds further confirms the presence of an interaction between PANI and the TiO_2 hollow spheres.

The optical properties of TiO_2 hollow spheres, PANI, and TiO_2/PANI hybrids shown in Fig. 4 were measured by

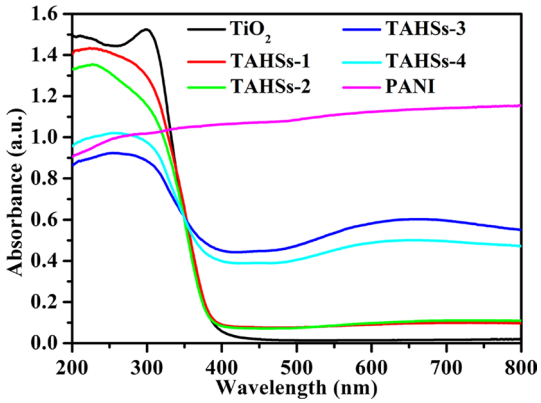

Fig. 4 UV–Vis diffuse reflectance spectra of TiO_2 hollow spheres, PANI, and TiO_2/PANI hybrid materials

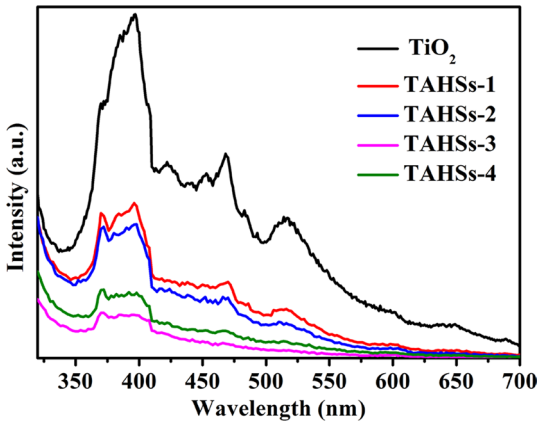

Fig. 5 PL spectra of TiO_2 hollow spheres and TiO_2/PANI hybrid materials

UV–Vis diffuse reflectance spectroscopy [44]. Pure TiO_2 can only absorb UV light at wavelengths below 400 nm [45, 46], whereas PANI can absorb both UV and visible light, by virtue of transitions from π to π^* levels in the PANI molecules [36]. Hence, the absorption range of the TiO_2/PANI hybrid materials is extended into the visible range as far as 800 nm, indicating that PANI acts as a photosensitizer for TiO_2. TiO_2/PANI hybrid materials can be induced to generate more electron–hole pairs via the absorption of both UV and visible light, which should improve their photocatalytic performance.

For semiconductor nanomaterials, photoluminescence spectroscopy (PL) can be used to evaluate the efficiency of trapping, migration, and separation of photogenerated charge carriers, since photocatalytic performance is related to both the PL intensity and separation of photogenerated electron–hole pairs [47]. In general, a higher PL intensity indicates lower separation and transfer efficiency of photogenerated electron–hole pairs, corresponding to a lower photocatalytic activity. PL spectra of our materials are shown in Fig. 5. It is seen that the PL intensity of TiO_2 hollow spheres is much higher than the TiO_2/PANI hybrids; the remarkable reduction of PL intensity for the latter implies a high separation efficiency of the charge carriers. The PL intensity decreases in the order: TiO_2 > TAHSs-1 > TAHSs-2 > TAHSs-4 > TAHSs-3, and hence TAHSs-3 should have the best electron–hole pairs separation.

Photocatalytic activity

As shown in Fig. 6, the photocatalytic activities of our samples were assessed by degradation of MO under both UV and visible light. Prior to irradiation, surface adsorption of MO on the surface of the samples is observed (Fig. 6a, b), although adsorption on the TiO_2 hollow spheres is much lower than that on the TiO_2/PANI hybrids. The adsorption was highest for TAHSs-3. Figure 6a, b show the photocatalytic degradation profiles of MO over the samples. The TiO_2 hollow spheres exhibit minimal photocatalytic activity compared to the TiO_2/PANI hybrids; the photocatalytic efficiency of the TiO_2 hollow spheres is approximately 55.8% after 2 h and 10.0% after 4 h under UV and visible light, respectively. These results are attributed to the wide bandgap of pure TiO_2, which requires UV light. The photocatalytic activity of TiO_2 increases with increasing TBT content (Fig. S7). For the hybrid materials, the PANI layer has a strong influence on the photocatalytic degradation of MO, such that the degradation efficiency initially increases with increasing PANI content. However, excess PANI content results in a decline of photocatalytic activity for TAHSs-4, presumably because the higher PANI content covers up the surface of the TiO_2 hollow spheres, preventing diffusion of MO to the TiO_2 layer. Overall, the photocatalytic activity follows the order TiO_2 < TAHSs-1 < TAHSs-2 < TAHSs-4 < TAHSs-3. For TAHSs-3, the photodegradation efficiencies are approximately 90.9% after 2 h under UV light and 97.1% after 4 h under visible light.

In order to better understand the photocatalysis of these materials, kinetic simulation of MO degradation was carried out as shown in Fig. 6c, d. Taking into consideration the low initial concentration of MO, the kinetic process was fitted using an apparent Langmuir–Hinshelwood first-order kinetic model, following the equation ($\ln C_0/C = kt$) [19]. The photocatalytic reaction rates follow the order TiO_2 < TAHSs-1 < TAHSs-2 < TAHSs-4 < TAHSs-3 under both UV and visible light, which is in accord with their photocatalytic activities (Fig. 6a, b).

The stabilities of the photocatalysts under UV and visible light were investigated, as shown in Fig. 6e, f. After recycling for four experiments, we observed no significant reduction in photocatalytic performance, indicating that

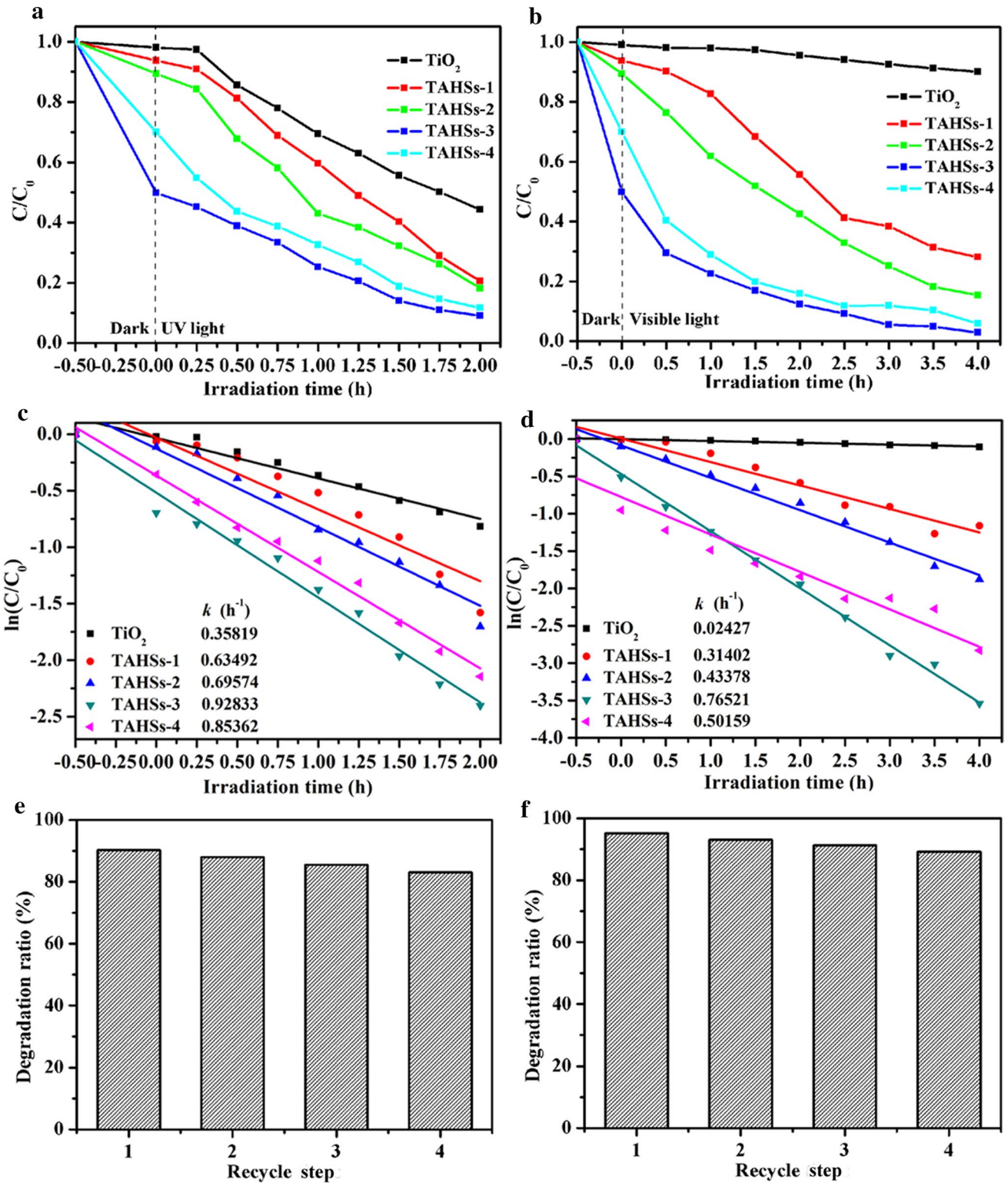

Fig. 6 **a**, **b** Photocatalytic degradation profiles and **c**, **d** kinetic linear simulation of MO over the samples, and **e**, **f** photocatalytic stability of TAHSs-3 under **a**, **c**, and **e** UV light and **b**, **d**, and **f** visible light

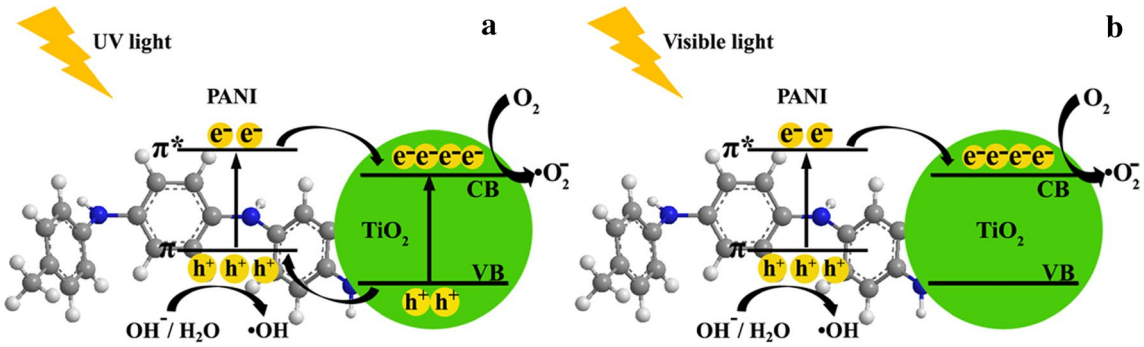

Scheme 2 Mechanism of photocatalytic degradation by TiO_2/PANI hollow spheres with double-shell structure under **a** UV light and **b** visible light

these hybrid materials have good stability and reusability, which is important for their practical application in wastewater treatment. In addition, there was no change in the XRD spectra of TAHSs-3 before and after MO degradation (Fig. S8), providing further evidence of its photocatalytic stability.

A plausible mechanism for photocatalytic degradation of MO by TiO_2/PANI hybrids is proposed in Scheme 2. The band gaps of TiO_2 and PANI are approximately 3.2 [6] and 2.8 eV [20], respectively. There should be a synergistic effect between TiO_2 and PANI, since the conduction band (CB) of TiO_2 matches well with the LUMO of PANI, whilst the valence band (VB) of TiO_2 matches well with the HOMO of PANI [48]. When exposed to UV light (Scheme 2a), both TiO_2 and PANI generate electron–hole pairs. Based on the synergistic effect, the LUMO electrons in PANI are transferred into the CB of the TiO_2, whilst photogenerated holes of the VB of TiO_2 can migrate to the HOMO of PANI. Under visible light (Scheme 2b), PANI can absorb photons to produce the π–π^* transition, such that electrons in the HOMO are excited into the LUMO [49]. These excited electrons can then readily transfer to the CB of the TiO_2. Charge transfer processes in the TiO_2/PANI hybrid materials thus promote separation of the photogenerated charge carriers, leading to the observed enhancement in photocatalytic activity. With respect to the photocatalytic degradation of MO, the excited electrons can be trapped by adsorbed molecular oxygen, giving superoxide anion radicals ($\cdot O_2^-$). Meanwhile, hydroxyl radicals ($\cdot$OH) can also be formed by reaction of the holes with water or hydroxide ions. Both of these radicals can react with MO.

Conclusion

In summary, double-shell structured TiO_2/PANI hollow spheres were synthesized by sol–gel and in situ polymerization processes. The shell thickness can be adjusted by varying the precursor concentration. Based on the photocatalytic degradation of MO, these TiO_2/PANI hybrid materials show significant photocatalytic activities. The TiO_2/PANI hollow spheres with optimized PANI content gave maximum photocatalytic efficiencies of 90.9% and 97.1% under UV and visible light, respectively. We believe that this study may be helpful for construction of other conducting polymers and TiO_2 hybrid materials with a view to their potential application in wastewater treatment.

Acknowledgements This work was supported by the National Natural Science Foundation of China (Grant Nos. 51572134, 51372124, 51503108) and the Program for Scientific Research Innovation Team in Colleges and Universities of Shandong Province.

References

1. Sun B, Zhou GW, Shao CW, Jiang B, Pang JL, Zhang Y (2014) Spherical mesoporous TiO_2 fabricated by sodium dodecyl sulfate-assisted hydrothermal treatment and its photocatalytic decomposition of papermaking wastewater. Powder Technol 256:118–125
2. Yang J, Jiang YL, Li LJ, Muhire E, Gao MZ (2016) High-performance photodetectors and enhanced photocatalysts of two-dimensional TiO_2 nanosheets under UV light excitation. Nanoscale 8:8170–8177
3. Li HL, Yu QJ, Huang YW, Yu CL, Li RZ, Wang JZ, Guo FY, Zhang Y, Zhang XT, Wang P, Zhao LC (2016) Ultralong rutile TiO_2 nanowire arrays for highly efficient dye-sensitized solar cells. ACS Appl Mater Interfaces 8:13384–13391
4. Perera SD, Mariano RG, Vu K, Nour N, Seitz O, Chabal Y Jr, Balkus KJ Jr (2012) Hydrothermal synthesis of graphene-TiO_2 nanotube composites with enhanced photocatalytic activity. ACS Catal 2:949–956
5. Jia CC, Yang P, Chen HS, Wang JP (2015) Template-free synthesis of mesoporous anatase titania hollow spheres and their enhanced photocatalysis. CrystEngComm 17:2940–2948
6. Wang Y, Zheng YZ, Lu SQ, Tao X, Che Y, Chen JF (2015) Visible-light-responsive TiO_2-coated ZnO: I nanorod array films with enhanced photoelectrochemical and photocatalytic performance. ACS Appl Mater Interfaces 7:6093–6101
7. Sohn H, Kim SY, Shin WH, Lee JM, Lee H, Yun DJ, Moon KS, Han I, Kwak C, Hwang SJ (2018) Novel flexible transparent conductive films with enhanced chemical and electromechanical

sustainability: TiO_2 nanosheet–Ag nanowire hybrid. ACS Appl Mater Interfaces 10:2688–2700
8. Talebi SMS, Kazeminezhad I, Motamedi H (2018) TiO_2 hollow spheres as a novel antibiotic carrier for the direct delivery of gentamicin. Ceram Int 44:13457–13462
9. Li J, Qin Y, Jin C, Li Y, Shi DL, Mende LS, Gan LH, Yang JH (2013) Highly ordered monolayer/bilayer TiO_2 hollow sphere films with widely tunable visible–light reflection and absorption bands. Nanoscale 5:5009–5016
10. Khojasteh H, Niasari MS, Sangsefidi FS (2018) Photocatalytic evaluation of RGO/TiO_2NWs/Pd–Ag nanocomposite as an improved catalyst for efficient dye degradation. J Alloys Compd 746:611–618
11. Hoseinzadeh T, Solaymani S, Kulesza S, Achour A, Ghorannevis Z, Talu S, Bramowicz M, Ghoranneviss M, Rezaee S, Boochani A, Mozaffari N (2018) Microstructures, fractal geometry and dye-sensitized solar cells performance of CdS/TiO_2 nanostructures. J Electroanal Chem 830–831:80–87
12. Dantan D, Gosavi SW, Chaure NB (2015) Studies on electrical properties of hybrid polymeric gate dielectric for field effect transistors. Macromol Symp 347:81–86
13. Dastan D, Banpurkar A (2017) Solution processable sol–gel derived titania gate dielectric for organic field effect transistors. J Mater Sci Mater Electron 28:3851–3859
14. Zhou J, Ren F, Zhang SF, Wu W, Xiao XH, Liu Y, Jiang CZ (2013) SiO_2–Ag–SiO_2–TiO_2 multi-shell structures: plasmon enhanced photocatalysts with wide-spectral-response. J Mater Chem A 1:13128–13138
15. Wang MG, Hu YM, Han J, Guo R, Xiong HX, Yin YD (2015) TiO_2/NiO hybrid shells: p–n junction photocatalysts with enhanced activity under visible light. J Mater Chem A 3:20727–20735
16. Hao RR, Wang GH, Tang H, Sun LL, Xu C, Han DY (2016) Template-free preparation of macro/mesoporous g-C_3N_4/TiO_2 heterojunction photocatalysts with enhanced visible light photocatalytic activity. Appl Catal B 187:47–58
17. Minella M, Bertaina F, Minero C (2018) The complex interplay between adsorption and photoactivity in hybrids rGO/TiO_2. Catal Today 315:9–18
18. Chen J, Wang N, Ma HY, Zhu JW, Feng JT, Yan W (2017) Facile modification of a polythiophene/TiO_2 composite using surfactants in an aqueous medium for an enhanced Pb(II) adsorption and mechanism investigation. J Chem Eng Data 62:2208–2221
19. Lin YM, Li DZ, Hu JH, Xiao GG, Wang JX, Li WJ, Fu XZ (2012) Highly efficient photocatalytic degradation of organic pollutants by PANI-modified TiO_2 composite. J Phys Chem C 116:5764–5772
20. Chen X, Li HK, Wu HS, Wu YX, Shang YY, Pan J, Xiong X (2016) Fabrication of TiO_2@PANI nanobelts with the enhanced absorption and photocatalytic performance under visible light. Mater Lett 172:52–55
21. Razak S, Nawi MA, Haitham K (2014) Fabrication, characterization and application of a reusable immobilized TiO_2–PANI photocatalyst plate for the removal of reactive red 4 dye. Appl Surf Sci 319:90–98
22. Palmas S, Mascia M, Vacca A, Llanos J, Mena E (2014) Analysis of photocurrent and capacitance of TiO_2 nanotube–polyaniline hybrid composites synthesized through electroreduction of an aryldiazonium salt. RSC Adv 4:23957–23965
23. Youssef A (2014) Morphological studies of polyaniline nanocomposite based mesostructured TiO_2 nanowires as conductive packaging materials. RSC Adv 4:6811–6820
24. Zhang L, Chen L, Qi B, Yang GC, Gong J (2015) Synthesis of vertical aligned TiO_2@polyaniline core–shell nanorods for high-performance supercapacitors. RSC Adv 5:1680–1683
25. Xiang YQ, Li YY, Zhang XT, Zhou AN, Jing N, Xu QH (2017) Hybrid Cu_xO–TiO_2 porous hollow nanospheres: preparation, characterization and photocatalytic properties. RSC Adv 7:31619–31627
26. Deng YC, Tang L, Zeng GM, Dong HR, Yan M, Wang JJ, Hu W, Wang JJ, Zhou YY, Tang J (2016) Enhanced visible light photocatalytic performance of polyaniline modified mesoporous single crystal TiO_2 microsphere. Appl Surf Sci 387:882–893
27. Zare M, Solaymani S, Shafiekhani A, Kulesza S, Talu S, Bramowicz M (2018) Evolution of rough-surface geometry and crystalline structures of aligned TiO_2 nanotubes for photoelectrochemical water splitting. Sci Rep 8:1–11
28. Pouget JP, Jozefowicz ME, Epstein AJ, Tang X, Macdiarmid AG (1991) X-ray structure of polyaniline. Macromolecules 24:779–789
29. Lai C, Zhang HZ, Li GR, Gao XP (2011) Mesoporous polyaniline/TiO_2 microspheres with core–shell structure as anode materials for lithium ion battery. J Power Sources 196:4735–4740
30. Terohid SAA, Heidari S, Jafari A, Aagary S (2018) Effect of growth time on structural, morphological and electrical properties of tungsten oxide nanowire. Appl Phys A 124:567(1)–567(9)
31. Dastan D (2015) Nanostructured anatase titania thin films prepared by sol–gel dip coating technique. J At Mol Condens Nano Phys 2:109–114
32. Achour A, Chaker M, Achour H, Arman A, Islam M, Mardani M, Boujtita M, Brizoual LL, Djouadi MA, Brousse T (2017) Role of nitrogen doping at the surface of titanium nitride thin films towards capacitive charge storage enhancement. J Power Sources 359:349–354
33. Wang ZM, Peng XY, Huang CY, Chen X, Dai WX, Fu XZ (2017) CO gas sensitivity and its oxidation over TiO_2 modified by PANI under UV irradiation at room temperature. Appl Catal B 219:379–390
34. Dastan D, Chaure N, Kartha M (2017) Surfactants assisted solvothermal derived titania nanoparticles: synthesis and simulation. J Mater Sci Mater Electron 28:7784–7796
35. Dastan D, Panahi SL, Chaure NB (2016) Characterization of titania thin films grown by dip-coating technique. J Mater Sci Mater Electron 27:12291–12296
36. Zhang LX, Liu P, Su ZX (2006) Preparation of PANI–TiO_2 nanocomposites and their solid-phase photocatalytic degradation. Polym Degrad Stab 91:2213–2219
37. Niu Z, Yang Z, Hu Z, Lu Y, Han CC (2003) Polyaniline–silica composite conductive capsules and hollow spheres. Adv Funct Mater 13:949–954
38. Dastan D (2017) Effect of preparation methods on the properties of titania nanoparticles: solvothermal versus sol–gel. Appl Phys A 123:699(1)–699(13)
39. Kim BS, Lee KT, Huh PH, Lee DH, Jo NJ, Lee JO (2009) In situ template polymerization of aniline on the surface of negatively charged TiO_2 nanoparticles. Synth Met 159:1369–1372
40. Liao GZ, Chen S, Quan X, Zhang YB, Zhao HM (2011) Remarkable improvement of visible light photocatalysis with PANI modified core–shell mesoporous TiO_2 microspheres. Appl Catal B 102:126–131
41. Chen M, Wang M, Yang ZY, Wang XD (2017) High performance and durability of order-structured cathode catalyst layer based on TiO_2@PANI core-shell nanowire arrays. Appl Surf Sci 406:69–76
42. Wen T, Fan QH, Tan XL, Chen YT, Chen CL, Xu AW, Wang XK (2016) A core–shell structure of polyaniline coated protonic titanate nanobelt composites for both Cr(VI) and humic acid removal. Polym Chem 7:785–794
43. Guo N, Liang YM, Lan S, Liu L, Zhang JJ, Ji GJ, Gan SC (2014) Microscale hierarchical three-dimensional flowerlike TiO_2/PANI composite: synthesis, characterization, and its remarkable

photocatalytic activity on organic dyes under UV-light and sunlight irradiation. J Phys Chem C 118:18343–18355
44. Alavi A, Jafari A, Heidary S, Fayaz V, Terohid SAA (2018) Effect of laser pulse energy on the structure, morphology and optical properties of tantalum-oxide nanoparticles generated by laser ablation. J Nanoelectron Optoelectron 13:1407–1412
45. Dastan D, Panahi SL, Yengntiwar AP, Banpurkar AG (2016) Morphological and electrical studies of titania powder and films grown by aqueous solution method. Adv Sci Lett 22:950–953
46. Korpi ARG, Luna C, Arman A, Talu S (2017) Influence of the oxygen partial pressure on the growth and optical properties of RF-sputtered anatase TiO_2 thin films. Results Phys 7:3349–3352
47. Ansari MO, Khan MM, Ansari SA, Raju K, Lee J, Cho MH (2014) Enhanced thermal stability under DC electrical conductivity retention and visible light activity of Ag/TiO_2@polyaniline nanocomposite film. ACS Appl Mater Interfaces 6:8124–8133
48. Radoicic M, Saponjic Z, Jankovic IA, Marjanovic GC, Ahrenkielc SP, Comor MI (2013) Improvements to the photocatalytic efficiency of polyaniline modified TiO_2 nanoparticles. Appl Catal B 136–137:133–139
49. Zhang LJ, Wan MX (2003) Polyaniline/TiO_2 composite nanotubes. J Phys Chem B 107:6748–6753